

Fast degradation of azo dye by nanocrystallized Fe-based alloys

[Wang PeiPei](#), [Wang JunQiang](#), [Huo JunTao](#), [Xu Wei](#), [Wang XinMin](#) and [Wang Gang](#)

Citation: [SCIENCE CHINA Physics, Mechanics & Astronomy](#) **60**, 076112 (2017); doi: 10.1007/s11433-017-9034-5

View online: <http://engine.scichina.com/doi/10.1007/s11433-017-9034-5>

View Table of Contents: <http://engine.scichina.com/publisher/scp/journal/SCPMA/60/7>

Published by the [Science China Press](#)

Articles you may be interested in

[Rapid reductive degradation of azo dyes by a unique structure of amorphous alloys](#)

Chinese Science Bulletin **56**, 3988 (2011);

[NEW LEVEL OF MAGNETIC PROPERTIES OF NEW Fe-BASED MICROCRYSTALLINE ALLOYS](#)

Chinese Science Bulletin **37**, 790 (1992);

[Rapid decolorization of water soluble azo-dyes by nanosized zero-valent iron immobilized on the exchange resin](#)

Science in China Series B-Chemistry **51**, 186 (2008);

[INVESTIGATION ON AMORPHOUS Fe-BASED ALLOYS WITH HIGH INITIAL PERMEABILITY AND LOW COERCIVE FORCE](#)

Chinese Science Bulletin **36**, 700 (1991);

[COLOUR SYSTEMS OF MIXED POLYNUCLEAR COMPLEXES OF LANTHANUM-2,7-BISAZOCHROMOTROPIC ACID DYES-ZINC-O-PHENANTHROLINE](#)

Chinese Science Bulletin **35**, 1440 (1990);

Fast degradation of azo dye by nanocrystallized Fe-based alloys

PeiPei Wang^{1,2}, JunQiang Wang^{2*}, JunTao Huo², Wei Xu², XinMin Wang², and Gang Wang^{1*}

¹ School of Materials Science and Engineering, Shanghai University, Shanghai 200444, China;

² CAS Key Laboratory of Magnetic Materials and Devices & Zhejiang Province Key Laboratory of Magnetic Materials and Application Technology, Ningbo Institute of Materials Technology & Engineering, Chinese Academy of Sciences, Ningbo 315201, China

Received March 14, 2017; accepted April 05, 2017; published online May 17, 2017

Exploring new alloys with high efficiency in degrading organic pollutants in aqueous solutions is of wide interests. Here, we report that the nanocrystallized Fe_{82.65}Si₄B₁₂Cu_{1.35} alloy exhibits higher efficiency in decolorizing azo dye solutions compared to its amorphous counterpart. The increased efficiency is attributed to the formation of numerous microbatteries between the α -Fe(Si) and Fe₂B nanocrystalline phases, which exhibit different corrosion potentials. These results suggest that nanocrystallized Fe-based amorphous composites hold promising application potential in degrading azo dyes solutions.

nanocrystalline alloys, amorphous alloys, degradation of azo dye

PACS number(s): 81.05.Kf, 65.60.+a, 82.80.Fk, 61.10.-i

Citation: P. P. Wang, J. Q. Wang, J. T. Huo, W. Xu, X. M. Wang, and G. Wang, Fast degradation of azo dye by nanocrystallized Fe-based alloys, *Sci. China-Phys. Mech. Astron.* **60**, 076112 (2017), doi: 10.1007/s11433-017-9034-5

1 Introduction

Due to their far-from-equilibrium nature [1,2], many amorphous alloys, such as Fe-based [3-10], Mg-based [11-16], Al-based [17], and Co-based alloys [18], exhibit advanced properties in degrading azo dye solutions. Among these alloys, Fe-based alloys have attracted wide interests because of high reaction efficiency and cheap price. The chemical and physical properties of amorphous crystalline composite materials can be enhanced greatly via tuning and designing the type, size, number, and distribution of the crystalline phases in the amorphous matrix [19-22]. For example, the fine and uniform distribution of α -Fe in the Fe-based amorphous alloys can further enhance the soft magnetic properties, i.e. increase saturation magnetic flux density B_s [23,24]. It is interesting to check whether the degradation efficiency can be

further increased by modifying the structure amorphous alloys.

In this work, we studied the reactivity of both the as-quenched (amorphous) and annealed (nanocrystalline) Fe_{82.65}Si₄B₁₂Cu_{1.35} ribbons in degrading Direct Blue (DB) 2B azo dye solutions. It is surprising that the reactivity of the crystallized ribbons is much higher than that of amorphous ribbons. The reaction mechanism has been studied based on the potentiodynamic polarization curves in azo dye solutions and surface morphologies of the reacted ribbons.

2 Experimental

2.1 Fabrication and characterization

The alloy ingots with nominal composition of Fe_{82.65}Si₄B₁₂Cu_{1.35} (FeSiBCu) were prepared by induction melting the mixtures of pure Fe, Si, B, Cu under protection of high purity argon. The FeSiBCu amorphous ribbons with

*Corresponding authors (JunQiang Wang, email: jqwang@nimte.ac.cn; Gang Wang, email: g.wang@shu.edu.cn)

width of about 1.0 mm and thickness of about 0.02 mm were fabricated by single roller melt-spinning method under the protection of high purity argon. The surface speed of spinning roller is 45 m/s. The Curie temperature (T_c) and crystallization temperature (T_{x1} and T_{x2}) were measured by differential scanning calorimetry (DSC, Netzsch 404C, Germany) at a heating rate of 0.67 K/s. To obtain nanocrystallized samples, the as-quenched ribbons were annealed at 763 K for 5 min in vacuum (10^{-3} Pa) using a tube furnace. The atomic structures of the as-quenched and annealed ribbons were characterized using X-ray diffraction (XRD, Bruker D8 Advance, Germany) with Cu $K\alpha$ radiation. The fracture morphologies of the ribbons were observed using scanning electron microscopy (SEM, Hitachi S4800, Japan).

2.2 Reactivity Measurements

Azo dye ($C_{32}H_{20}N_6Na_4O_{14}S_4$, direct blue 2B, hereafter named as DB 2B) powders of high quality were purchased from Shanghai East Lion Silk Screen Printing Ink Co., Ltd (China). Dye solution with a concentration of 200 mg/L was prepared by dissolving the azo dye powders with deionized water. For each time, a volume of 70 mL of DB 2B solution was put into the 100 mL beaker for reaction test. The temperature was controlled at 30 °C by water-bath device. The FeSiBCu metallic ribbons were cut into small parts with a size of 10 mm × 1.0 mm × 0.02 mm with a specific surface area of about 0.016 m²/g. Then, the ribbons were put into the solution with a ratio of 10 g/L. The solution was not stirred during

degradation. 2 mL solution was extracted each time for ultra-violet-visible absorption spectrophotometer (Perkin-Elmer Lambda 950, USA) test to measure the concentration decay of solutions.

2.3 Mechanism analysis

Potentiodynamic polarization curves were measured at a scanning rate of 20 mV/s using electrochemical work station (Zahner Zennium, Germany) in azo dye solution at room temperature. Three-electrode method was used to measure the electrochemical properties, with the samples acting as the working electrode, the saturated calomel electrode (SCE) as the reference electrode, and a platinum sheet as the counter electrode. Before electrochemical tests, all samples were polished with metallographic sandpaper of 1500 grit, and washed by ethanol. The surface morphologies of the ribbons after reaction were observed by scanning electron microscopy (SEM, Hitachi S4800, Japan).

3 Results

3.1 Characterization of the FeSiBCu metallic ribbons

Thermal parameters of as-quenched FeSiBCu ribbons were measured by DSC. As shown in Figure 1(a), The Curie temperature T_c is 598 K. The first crystallization temperature T_{x1} is 668 K, which is related to the precipitation of α -Fe(Si) [25].

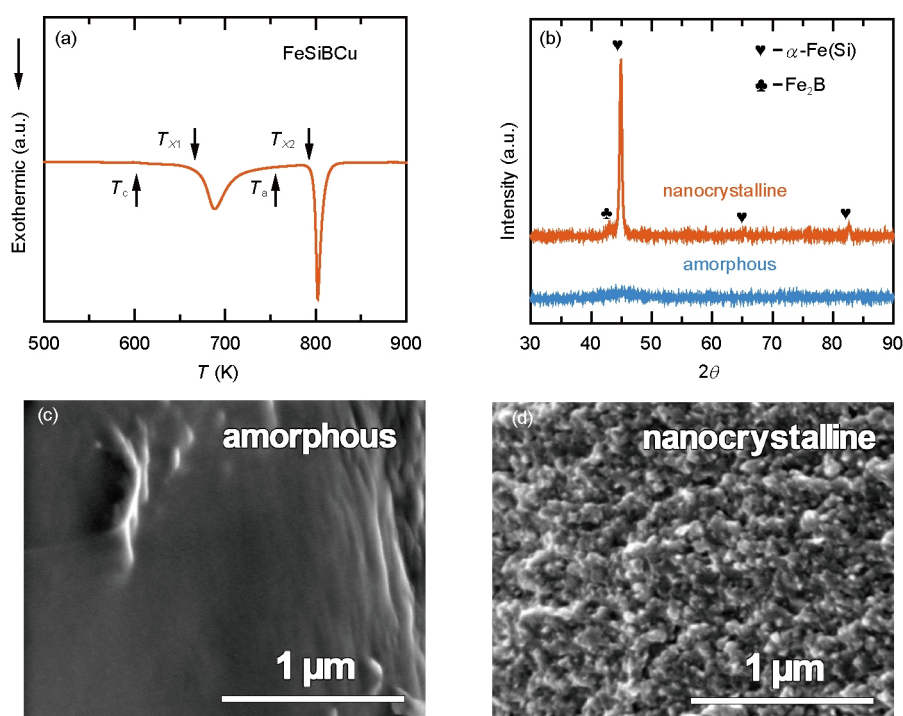


Figure 1 (Color online) (a) DSC trace of as-spun FeSiBCu ribbon at a heating rate of 0.67 K/s; (b) XRD curves of the FeSiBCu ribbons confirm the nanocrystalline structure after being annealed at 763 K for 5 min; cross section morphologies of amorphous (c) and nanocrystalline (d) FeSiBCu ribbons.

The second crystallization temperature T_{x2} is 794K, which is ascribed to the precipitation of Fe_2B and other new phases [26,27]. The annealing temperature T_a is 763K, right between T_{x1} and T_{x2} , much more close to T_{x2} . The atomic structure of as-quenched and annealed FeSiBCu ribbons was investigated by XRD. As shown in Figure 1(b), for the as-quenched ribbons, the XRD curve exhibits broad diffusive diffraction peak which confirms the amorphous nature of the ribbon. For the annealed ribbons, Bragg peaks corresponding to nanosized $\alpha\text{-Fe}$ and Fe_2B can be found. The grain size of the nanocrystalline is about 10nm for Fe_2B , 24nm for $\alpha\text{-Fe}$, which is estimated by the full width of half maximum of the diffraction peak at $2\theta=43.0^\circ$ and 44.8° , respectively. Figure 1(c) and (d) shows the morphologies of the fracture surface for the two ribbons. For the as-quenched ribbons, the fracture surface is very smooth, which demonstrates the amorphous structure of the as-quenched ribbons, as shown in Figure 1(c). For the annealed ribbons, nano particles that are distributed uniformly are observed, which confirms the precipitation of nanosized $\alpha\text{-Fe}(\text{Si})$ and Fe_2B , as shown in Figure 1(d).

3.2 Decolorization by FeSiBCu ribbons

To evaluate the decolorization efficiency of nanocrystallized Fe-based ribbons, the degradation experiments were carried out with amorphous and nanocrystallized FeSiBCu ribbons, respectively. The UV absorption spectra are shown in Figure 2(a). The characteristic absorption peak around 570nm arises from -N=N- of DB 2B dye molecules [4,6,28]. The intensity of the absorption peak is proportional to the concentration of azo dye solution. Along with the degradation of azo dyes, the intensity of the absorption peak decreases. The change of normalized concentration of DB 2B solutions is shown in Figure 2(b). It is clear that the concentration of azo dye solution decays faster when using nanocrystallized ribbons than amorphous ribbons. The degradation process is fitted using a pseudo first-order reaction equation, $C = C_1 \exp(-t/t_0) + C_2$, where C is the normalized concentration of solution, C_1 and C_2 are fitting constants, t is reaction time, t_0 is degradation time constant. The comparison of t_0 for the amorphous and nanocrystallized FeSiBCu ribbons is shown in Figure 2(c). For amorphous ribbons, $t_0=142\text{min}$. For nanocrystallized ribbons, $t_0=114\text{min}$. Thus, the degradation efficiency of nanocrystallized ribbons increases by about 20% ($\Delta t=28\text{min}$) than that of amorphous ribbons.

4 Discussion

4.1 Electrochemical characterization

To distinguish the difference in reaction kinetics between amorphous and nanocrystallized FeSiBCu ribbons, potenti-

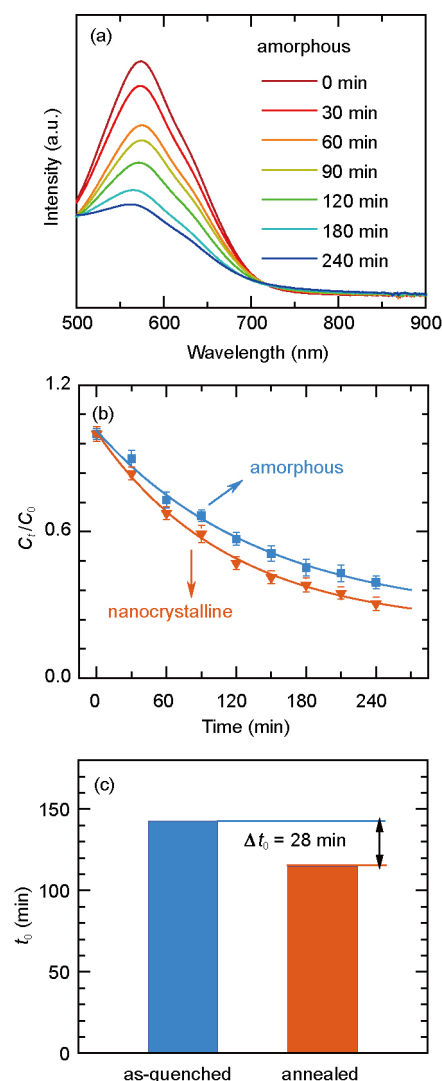


Figure 2 (Color online) (a) The UV absorption spectra of DB 2B solution after different reaction time with FeSiBCu amorphous ribbons; (b) the normalized concentration of DB 2B solution after different degradation time with FeSiBCu ribbons, the solid curves are fitting results by $C = C_1 \exp(-t/t_0) + C_2$; (c) the comparison of degradation time constant t_0 for the amorphous and nanocrystallized FeSiBCu ribbons.

dynamic polarization curves were measured in azo dye solutions, as shown in Figure 3. For the amorphous ribbons, the corrosion potential is about -0.81V . For the nanocrystallized ribbons, besides the primary corrosion potential at about -0.87V , there exists another secondary corrosion potential at about -0.62V . The primary corrosion potential at -0.87V , which is smaller than the amorphous ribbons, is attributed to the corrosion of $\alpha\text{-Fe}(\text{Si})$. The corrosion potential at -0.62V can be ascribed to the corrosion of Fe_2B . The mismatch in corrosion potentials for different phases will form microbattery. Thus, due to the micro-battery effect, the zero valent iron Fe^0 in $\alpha\text{-Fe}(\text{Si})$ becomes more easier to donate its electrons to N=N bond, and the azo dye solution gets decolorized much faster. This is also confirmed by the larger corrosion density for the nanocrystallized sample.

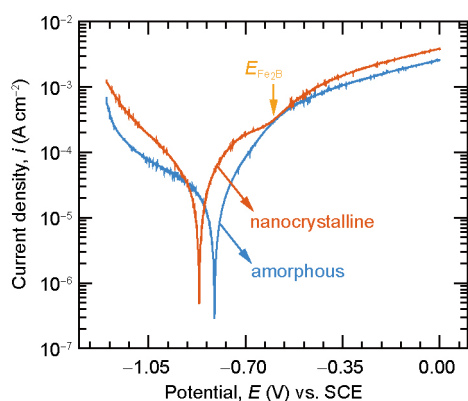


Figure 3 (Color online) Potentiodynamic polarization curves of amorphous and nanocrystallized FeSiBCu ribbons in azo dye solutions.

It has been widely observed that amorphous alloys exhibit much higher decolorization efficiency compared to their crystalline counterparts [3,11,18,29,30], which are attributed to the metastable nature of amorphous structure. In these cases, the crystalline alloys were usually prepared by annealing amorphous ribbons at very high temperature for long time. In such a case, the crystal will grow very large which will not benefit the reaction with azo dye solution. The nanocrystallized samples are composed of numerous microbatteries as active sites for degradation of azo dyes.

4.2 Surface morphology

To further confirm the hypothesis of the formation of microbatteries, surface morphologies for the two FeSiBCu ribbons after reaction with DB 2B solutions were observed, as shown in Figure 4(a) and (b). For the amorphous ribbons, the number of corrosion pits is small and the corrosion pits are distributed in network, as shown in Figure 4(a). For the nanocrystallized ribbons, the number of corrosion pits is much larger and distributed dispersively and homogeneously, as shown in Figure 4(b). This suggests that the nanosized Fe₂B with high corrosion potential and the rest phases (α -Fe(Si) and amorphous matrix) with low corrosion potential form many micro-batteries with high reactivity. According to the above results, a schematic illustration of the degradation of azo dyes on the surface of nanocrystallized FeSiBCu ribbons were provided, as shown in Figure 5.

5 Conclusions

Fe-based nanocrystalline composite ribbons were fabricated by annealing the amorphous FeSiBCu ribbons at medium temperature. The decolorization efficiency of azo dyes increases by about 20% for nanocrystalline ribbons than amorphous ribbons. This is distinct from the conventional crystallized sample, where the grain size is very large. The

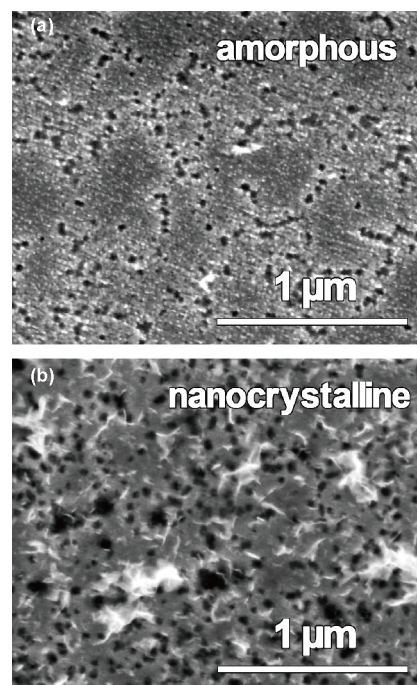


Figure 4 Surface morphologies of amorphous (a) and nanocrystallized (b) FeSiBCu ribbons after reaction with DB 2B solutions.

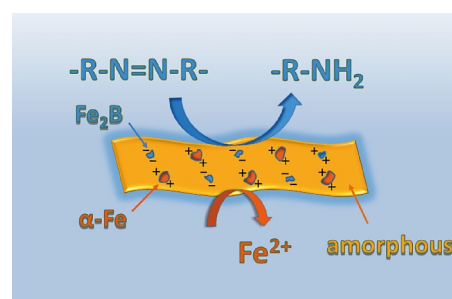


Figure 5 (Color online) Schematic illustration of the degradation of azo dyes on the surface of nanocrystallized FeSiBCu ribbons.

enhanced decolorization efficiency by nanocrystallized samples is attributed to the formation of numerous microbatteries formed by the different nanocrystals, which is confirmed by the electrochemical analysis and nanostructure of reacted sample. These results suggest that nanocrystalline Fe-based alloys hold promising potential in degrading azo dyes in aqueous solutions.

This work was supported by the National Natural Science Foundation of China (Grant No. 11504931), Ningbo Municipal Natural Science Foundation of China (Grant Nos. 2015A610064, 2015A610065, and 2015A610005), and One Hundred Talents Program of Chinese Academy of Sciences.

- 1 S. Singh, M. D. Ediger, and J. J. de Pablo, *Nat. Mater.* **12**, 139 (2013).
- 2 H. B. Yu, Y. Luo, and K. Samwer, *Adv. Mater.* **25**, 5904 (2013).
- 3 C. Zhang, H. Zhang, M. Lv, and Z. Hu, *J. Non-Crystal. Solid.* **356**, 1703 (2010).
- 4 J. Q. Wang, Y. H. Liu, M. W. Chen, G. Q. Xie, D. V.

- Louzguine-Luzgin, A. Inoue, and J. H. Perepezko, *Adv. Funct. Mater.* **22**, 2567 (2012).
- 5 P. Liu, J. L. Zhang, M. Q. Zha, and C. H. Shek, *ACS Appl. Mater. Interf.* **6**, 5500 (2014).
- 6 Y. Tang, Y. Shao, N. Chen, and K. F. Yao, *RSC Adv.* **5**, 6215 (2015).
- 7 Z. Jia, S. X. Liang, W. C. Zhang, W. M. Wang, C. Yang, and L. C. Zhang, *J. Taiwan Inst. Chem. Eng.* **71**, 128 (2017).
- 8 Z. Jia, W. C. Zhang, W. M. Wang, D. Habibi, and L. C. Zhang, *Appl. Catal. B Environ.* **192**, 46 (2016).
- 9 Z. Jia, X. Duan, W. Zhang, W. Wang, H. Sun, S. Wang, and L. C. Zhang, *Sci. Rep.* **6**, 38520 (2016).
- 10 Z. Jia, J. Kang, W. C. Zhang, W. M. Wang, C. Yang, H. Sun, D. Habibi, and L. C. Zhang, *Appl. Catal. B-Environ.* **204**, 537 (2017).
- 11 J. Q. Wang, Y. H. Liu, M. W. Chen, D. V. Louzguine-Luzgin, A. Inoue, and J. H. Perepezko, *Sci. Rep.* **2**, 418 (2012).
- 12 X. Luo, R. Li, J. Zong, Y. Zhang, H. Li, and T. Zhang, *Appl. Surf. Sci.* **305**, 314 (2014).
- 13 Z. Deng, C. Zhang, and L. Liu, *Intermetallics* **52**, 9 (2014).
- 14 Y. F. Zhao, J. J. Si, J. G. Song, Q. Yang, and X. D. Hui, *Mater. Sci. Eng. B* **181**, 46 (2014).
- 15 M. Iqbal, and W. H. Wang, *IOP Conf. Ser. Mater. Sci. Eng.* **60**, 012035 (2014).
- 16 M. Ramya, M. Karthika, R. Selvakumar, B. Raj, and K. R. Ravi, *J. Alloys Compd.* **696**, 185 (2017).
- 17 S. Das, S. Garrison, and S. Mukherjee, *Adv. Eng. Mater.* **18**, 214 (2016).
- 18 X. D. Qin, Z. W. Zhu, G. Liu, H. M. Fu, H. W. Zhang, A. M. Wang, H. Li, and H. F. Zhang, *Sci. Rep.* **5**, 18226 (2016).
- 19 M. E. McHenry, M. A. Willard, and D. E. Laughlin, *Prog. Mater. Sci.* **44**, 291 (1999).
- 20 C. Fan, and A. Inoue, *Appl. Phys. Lett.* **77**, 46 (2000).
- 21 D. C. Hofmann, J. Y. Suh, A. Wiest, G. Duan, M. L. Lind, M. D. Demetriou, and W. L. Johnson, *Nature* **451**, 1085 (2008).
- 22 J. Qiao, H. Jia, and P. K. Liaw, *Mater. Sci. Eng. R. Rep.* **100**, 1 (2016).
- 23 G. Herzer, *Acta. Mater.* **61**, 718 (2013).
- 24 M. Ohta, and Y. Yoshizawa, *J. Magn. Magn. Mater.* **320**, e750 (2008).
- 25 J. Dai, Y. G. Wang, L. Yang, G. T. Xia, Q. S. Zeng, and H. B. Lou, *J. Alloys Compd.* **695**, 1266 (2017).
- 26 H. T. Zhou, Z. K. Zhao, X. Zhou, B. Yan, J. W. Zhong, and Q. B. Li, *J. Alloys Compd.* **475**, 706 (2009).
- 27 H. R. Lashgari, Z. Chen, X. Z. Liao, D. Chu, M. Ferry, and S. Li, *Mater. Sci. Eng.-A* **626**, 480 (2015).
- 28 Z. Y. Lv, X. J. Liu, B. Jia, H. Wang, Y. Wu, and Z. P. Lu, *Sci. Rep.* **6**, 34213 (2016).
- 29 Y. Tang, Y. Shao, N. Chen, X. Liu, S. Q. Chen, and K. F. Yao, *RSC Adv.* **5**, 34032 (2015).
- 30 S. Xie, P. Huang, J. J. Kruzic, X. Zeng, and H. Qian, *Sci. Rep.* **6**, 21947 (2016).